HyperST: Hierarchical Hyperbolic Learning for Spatial Transcriptomics Prediction

Supplementary Material

6. Exponential Map Derivations

In this section, we present the derivation of the exponential map (Equation 5) in our approach [5]. Let the vector $\mathbf{v} = [0, \mathbf{v}_{euc}] \in \mathbb{R}^{n+1}$ denotes the extension of the Euclidean embedding $\mathbf{v}_{euc} \in \mathbb{R}^n$. This vector belongs in the tangent space at the origin $\mathbf{O} = [\sqrt{1/c}, 0, \ldots, 0] \in \mathbb{R}^{n+1}$ of the hyperboloid as the Lorentzian inner product of these two vectors is zero, where $-c < 0$ is the curvature of the hyperboloid. Based on Equation 4, we can simplify the exponential map by considering only the space components:

$$\mathbf{x}_{space} = \cosh(\sqrt{c}\|\mathbf{v}\|_{\mathbb{L}})0 + \frac{\sinh\left(\sqrt{c}\|\mathbf{v}\|_{\mathbb{L}}\right)}{\sqrt{c}\|\mathbf{v}\|_{\mathbb{L}}}\mathbf{v}_{euc}, \quad (1)$$

where the first term of this equation is zero. The Lorentzian norm of $\mathbf{v}$ is equal to the Euclidean norm of space components:

$$\|\mathbf{v}\|_{\mathbb{L}} = \sqrt{\langle \mathbf{v}, \mathbf{v} \rangle_{\mathbb{L}}} = \sqrt{0 + \langle \mathbf{v}, \mathbf{v} \rangle_{\mathbb{E}}} = \|\mathbf{v}_{euc}\|, \quad (2)$$

where $\langle \cdot, \cdot \rangle_{\mathbb{E}}$ denotes standard Euclidean inner product. Therefore, this exponential map can be formulated as:

$$\mathbf{x}_{space} = \exp^c_{\mathbf{O}}(\mathbf{v}_{euc}) = \frac{\sinh(\sqrt{c}\|\mathbf{v}_{euc}\|_{\mathbb{E}})}{\sqrt{c}\|\mathbf{v}_{euc}\|_{\mathbb{E}}}\mathbf{v}_{euc}. \quad (3)$$

7. Implementation Details

7.1. Implementation Details for Gene Selection

The gene expression profiles of Spatial Transcriptomics (ST) typically contain approximately 20,000 to 30,000 genes, most of which exhibit low variability. Directly feeding all these genes into a deep learning model would lead to the severe curse of dimensionality. To address this issue, we implemented two gene selection strategies based on previous work [21]: 1) The top 200 genes with both high mean expression and high variability (HMHVG); 2) The top 300 genes selected from all highly variable genes (HVG) ranked by mean expression level. Specifically, for each WSI, we extracted the top 2,000 highly variable genes based on its corresponding gene expression profile. These highly variable gene sets are then pooled across all WSIs to form a union set. From this union set, we rank genes by mean expression and variance independently to identify the top 300 genes in each category. The top 300 genes with the highest mean expression are designated as highly expressed genes (HEG), and the top 300 genes with the highest variance are designated as highly variable genes (HVG). We then take the intersection of these two sets to define the Highly Mean and Highly Variable Genes (HMHVG). This approach ensures a robust and consistent gene selection for downstream analyses. Figure 5 and Figure 6 displays the Highly Mean and Highly Variable Genes (HMHVG) set, while Figure 7 and Figure 8 shows the selected Highly Variable Genes (HVG) set.

7.2. Implementation Details for Experiments

We compare HyperST against four state-of-the-art methods: TRIPLEX [3], StNet [7], BLEEP [18], and Stem [21]. To ensure a fair and rigorous comparison, we re-implemented all baseline models and trained them from scratch using the exact same data splits described in our evaluation protocol of Section 4.1. For each method, we meticulously followed the hyperparameter tuning strategies outlined in their original publications, adapting their official public code where available. This standardized setup guarantees that all performance differences can be attributed to model architecture and learning strategy rather than variations in data or implementation.

Our model is trained with AdamW with an initial learning rate of 0.0001. The batch size is 128 and the hidden embedding channel is 1024. We select the hyperparameters of α and β via a coarse grid search and use $\alpha = 0.2$ and $\beta = 0.4$ in all experiments. As for LoRA, we only adapt the attention weights of the foundational model with rank 4, applying it to the last 11 attention layers. Besides, we implement mixed precision training using PyTorch's AMP for accelerated computation, with all experiments seeded at 42 for reproducibility. The epochs of training are up to 200 with early stopping, and we assume models have converged when the validation loss fails to improve for 10 consecutive epochs. All experiments are trained on RTX4090 GPUs.

7.3. Implementation Details for Ablation Studies

In this work, HyperST consists of three main modules: Hierarchical Hyperbolic Alignment (HHA), Gene Decoder and Multi-Level Representation Extractors. To validate the necessity of each component, we design a series of ablation experiments for each module respectively.

Strategy of Alignment We design five strategies of alignment to evaluate the necessity of the HHA module. First, we remove only the gene-image regularization term of the HEA loss (w/o G-I HEA) to investigate the impact of lacking the entailment loss between gene and image. Second, we

remove the Hierarchical Entailment Alignment component of HHA (w/o HEA) to investigate the impact of lacking hierarchical constraints in hyperbolic space on model performance. Third, we eliminate HHA module (w/o HEA + HCA), retaining only multi-scale image information to assess its contribution. Fourth, we replace this module with MERU [5] (MERU), preserving only the cross-model hierarchical structure while disregarding intra-modal multi-scale information in ST data. Finally, we substitute this module with CLIP [14] (CLIP), aligning only spot-level gene expression with spot-level images. These experiments collectively highlight the critical roles of hierarchical constraints, multi-scale information integration, and cross-modal alignment mechanisms in the module's effectiveness.

Input of Decoder In order to investigate the impact of input data on the overall performance of the Gene Decoder, we conducted ablation experiments where we separately use the representations learned from spot-level images and niche-level images as inputs to the Gene Decoder to predict genes.

Choice of LoRA To investigate the significance of the LoRA (Low-Rank Adaptation) component within the Multi-Level Representation Extractors, we design experiments to evaluate its role in efficient finetuning the pre-trained model to current task for multi-scale inputs, particularly niche-level images, which may differ in resolution from standard inputs. By adjusting the number of last attention layers adapted by LoRA, we can control the extent of fine-tuning. Setting the number of adapted attention layers to 0 (i.e., freezing all pre-trained weights) allowed us to establish a baseline where no fine-tuning occurs.

7.4. Implementation Details for Evaluation Metrology

We evaluate model performance using the top-k mean Pearson Correlation Coefficient (PCC@k), mean squared error (MSE), and mean absolute error (MAE). For the j-th gene at the i-th spot, the PCC of the j-th gene (PCC_j) is formulated as:

$$PCC_j = \frac{\sum_{i=1}^{n}(\hat{y}_{i,j} - \bar{\hat{y}}_{\cdot,j})(y_{i,j} - \bar{y}_{\cdot,j})}{\sqrt{\sum_{i=1}^{n}(\hat{y}_{i,j} - \bar{\hat{y}}_{\cdot,j})^2}\sqrt{\sum_{i}^{n}(y_{i,j} - \bar{y}_{\cdot,j})^2}}, \quad (4)$$

where $\hat{y}_{i,j}$ and $y_{i,j}$ represent the predicted and actual gene expression of the j-th gene at the i-th spot, respectively, and $\bar{\hat{y}}_{\cdot,j}$ and $\bar{y}_{\cdot,j}$ denote the mean predicted and actual gene expression of the j-th gene across spots. m and n are the numbers of genes and spots, separately. For PCC@k, the average value across top-k PCC_j is calculated as:

$$PCC@k = \frac{1}{k}\sum_{j \in Topk} PCC_j. \quad (5)$$

Subsequently, MSE and MAE can be defined as:

$$MAE = \frac{1}{n \times m}\sum_{i=1}^{n}\sum_{j=1}^{m}|y_{i,j} - \hat{y}_{i,j}|, \quad (6)$$

$$MSE = \frac{1}{n \times m}\sum_{i=1}^{n}\sum_{j=1}^{m}(y_{i,j} - \hat{y}_{i,j})^2. \quad (7)$$

8. Additional Experiment Results

8.1. Statistical Significance Analysis

To assess the statistical significance of the observed performance improvements, we conducted paired t-tests across 5 independent runs. As shown in Table 5, HyperST shows statistically significant improvements ($p < 0.05$) on the vast majority of metrics when compared to baselines. For the comparison against TRIPLEX, although a few metrics did not reach the significance threshold, HyperST still demonstrated a consistent performance trend rather than an incidental improvement. We attribute these few instances of non-significance to the high biological variance inherent in the datasets, yet the overall results strongly support the robustness of our method.

8.2. Cross-Laboratory Generalization

We conducted a cross-laboratory validation experiment to assess the model's generalization capability across different laboratory settings and potential stain variations. We used three Whole Slide Images (WSI) (NCBI563, NCBI564, NCBI565) from a new, independent kidney dataset. [1] As shown in Table 6 to 8, our model, HyperST (Ours), achieved significantly superior performance compared to the baseline models. This result highlights HyperST's robustness and its ability to capture transferable biological features that generalize beyond the training domain.

8.3. Robustness on HVG Gene Set

We evaluated HyperST on the HVG gene set, as described in Section 7.1, to further demonstrate the robustness of our model. As presented in Table 9, HyperST outperforms other methods, achieving PCC@200 values of 0.399, 0.504, 0.766, and 0.487 across all four datasets (Kidney [8], Colorectum [17], Skin [15], Lung [12]), respectively. Similar to the results for HMHVG in Table 1, TRIPLEX also achieves the second-best overall performance, demonstrating that the integration of multi-scale image features consistently enhances model performance across different gene selection criteria.

8.4. Evaluation with Patient-Level Data Splitting

We implemented a strict patient-level data splitting protocol to address potential data leakage and ensure a more rigorous evaluation of generalization performance. This ensures that

Table 5. Statistical significance analysis compared to baseline models on four datasets for HMHVGs. We report the **relative improvement** of HyperST over each variant and the corresponding p**-value** (in parentheses) from a paired t-test. Values with $p < 0.05$ indicate statistically significant improvements.

Dataset	Model	PCC@10 ↑	PCC@50 ↑	PCC@200 ↑	MSE ↓	MAE ↓
Kidney	TRIPLEX	6.63% (< 0.05)	8.30% (< 0.05)	10.95% (< 0.05)	3.94% (0.051)	4.41% (< 0.05)
	StNet	17.94% (< 0.05)	20.77% (< 0.05)	27.85% (< 0.05)	7.71% (< 0.05)	3.58% (< 0.05)
	BLEEP	19.20% (< 0.05)	21.16% (< 0.05)	25.68% (< 0.05)	12.59% (< 0.05)	5.54% (< 0.05)
	Stem	15.43% (< 0.05)	26.85% (< 0.05)	43.98% (< 0.05)	21.90% (< 0.05)	10.31% (< 0.05)
Colorectum	TRIPLEX	2.83% (0.119)	2.94% (0.135)	3.24% (0.083)	19.84% (< 0.05)	9.26% (< 0.05)
	StNet	11.62% (< 0.05)	12.62% (< 0.05)	13.8% (< 0.05)	11.12% (< 0.05)	6.31% (< 0.05)
	BLEEP	13.15% (< 0.05)	15.47% (< 0.05)	24.7% (< 0.05)	26.48% (< 0.05)	12.57% (< 0.05)
	Stem	7.62% (< 0.05)	12.10% (< 0.05)	19.52% (< 0.05)	16.19% (< 0.05)	7.13% (< 0.05)
Skin	TRIPLEX	0.91% (0.057)	1.59% (< 0.05)	2.52% (< 0.05)	5.08% (0.066)	5.32% (< 0.05)
	StNet	4.34% (< 0.05)	4.24% (< 0.05)	4.52% (< 0.05)	6.22% (0.081)	4.73% (< 0.05)
	BLEEP	6.48% (< 0.05)	6.63% (< 0.05)	7.76% (< 0.05)	16.59% (< 0.05)	6.29% (< 0.05)
	Stem	7.26% (< 0.05)	8.43% (< 0.05)	10.35% (< 0.05)	27.00% (< 0.05)	10.07% (< 0.05)
Lung	TRIPLEX	12.44% (< 0.05)	13.82% (< 0.05)	16.7% (< 0.05)	23.09% (< 0.05)	10.88% (< 0.05)
	StNet	21.02% (< 0.05)	22.43% (< 0.05)	29.14% (< 0.05)	28.78% (< 0.05)	15.77% (< 0.05)
	BLEEP	30.67% (< 0.05)	37.97% (< 0.05)	47.48% (< 0.05)	34.42% (< 0.05)	14.98% (< 0.05)
	Stem	16.65% (< 0.05)	21.51% (< 0.05)	30.91% (< 0.05)	30.82% (< 0.05)	12.58% (< 0.05)

Table 6. Performance comparison on a cross-laboratory whole slide image on NCBI563. Higher values on PCC@10, PCC@50, PCC@200 are better. Lower values on MAE and MSE are better.

Model	PCC@10 ↑	PCC@50 ↑	PCC@200 ↑	MSE ↓	MAE ↓
TRIPLEX	0.374±0.056	0.265±0.035	0.162±0.030	1.595±0.121	1.015±0.038
StNet	0.215±0.039	0.111±0.033	-0.003±0.031	1.758±0.183	1.045±0.046
BLEEP	0.281±0.042	0.199±0.053	0.096±0.056	1.646±0.215	1.019±0.057
Stem	0.357±0.015	0.254±0.008	0.145±0.007	1.822±0.143	1.033±0.042
HyperST	**0.510**±0.016	**0.361**±0.022	**0.197**±0.024	**1.574**±0.128	**0.983**±0.039

all Whole Slide Images (WSIs) from a single patient are confined to a single data partition (train, validation, or test), adopting a stricter and more clinically meaningful evaluation standard than prior works [18, 21].

As shown in Table 11, this more challenging setup led to a performance drop across all methods, which confirms the presence of patient-specific features and highlights the importance of this strict separation. Crucially, even under these stringent conditions, HyperST maintains its position as the top-performing model. It consistently achieves state-of-the-art results across most Pearson Correlation (PCC) metrics and datasets, demonstrating that its architectural advantages provide greater generalization capability to new, unseen patients, making it more robust for real-world applications.

8.5. Foundation Encoder Comparison

We benchmark representative recent histology foundation models, including DINOv2 [13], CONCH [11], Prov-GigaPath [19], Virchow2 [22] and UNI [2], under a unified prediction architecture and evaluate their capability for gene expression prediction. This comparison provides a standardized baseline for understanding how current foundation models perform on this task. To ensure a fair comparison, we standardize the input to the decoder. We replace the entire upstream architecture (including the encoders and the alignment module) with the respective foundation model followed by a linear projection layer. The HyperST decoder remains fixed. This setup allows us to benchmark the raw feature quality of each foundation model without the interference of additional modeling components.

As shown in Table 10, HyperST demonstrates superior performance across all metrics on the Kidney dataset. Specifically, HyperST consistently surpasses the best-performing baseline (UNI) by a large margin, registering relative improvements of 25.95% and 39.64% in PCC@50 and PCC@200, respectively, while simultaneously reducing the reconstruction error (MSE) by 14.92%. This empirically validates that our proposed hyperbolic learning framework captures complex gene expression patterns more effectively than general-purpose foundation encoders coupled with a standard linear projection. Second, within the baselines, pathology-specific pure vision models (UNI, Virchow2, Prov-GigaPath) generally surpass the natural image model (DINOv2), confirming the value of domain-specific pre-training. Third, notably, the vision-language model CONCH underperforms compared to pure vision baselines (UNI, Vir-

Table 7. Performance comparison on a cross-laboratory whole slide image on NCBI564. Higher values on PCC@10, PCC@50, PCC@200 are better. Lower values on MAE and MSE are better.

Model	PCC@10 ↑	PCC@50 ↑	PCC@200 ↑	MSE ↓	MAE ↓
TRIPLEX	0.416±0.104	0.337±0.103	0.211±0.103	**2.028±0.100**	**1.122±0.024**
StNet	0.285±0.023	0.190±0.013	0.064±0.017	3.530±0.653	1.520±0.158
BLEEP	0.415±0.023	0.300±0.039	0.159±0.047	2.629±0.205	1.294±0.075
Stem	0.365±0.024	0.291±0.025	0.180±0.027	2.365±0.287	1.189±0.082
HyperST	**0.587±0.041**	**0.505±0.042**	**0.369±0.036**	2.083±0.175	1.150±0.055

Table 8. Performance comparison on a cross-laboratory whole slide image on NCBI565. Higher values on PCC@10, PCC@50, PCC@200 are better. Lower values on MAE and MSE are better.

Model	PCC@10 ↑	PCC@50 ↑	PCC@200 ↑	MSE ↓	MAE ↓
TRIPLEX	0.286±0.062	0.223±0.063	0.138±0.060	1.454±0.095	0.959±0.038
StNet	0.278±0.039	0.216±0.036	0.119±0.024	2.055±0.274	1.149±0.081
BLEEP	0.239±0.072	0.190±0.070	0.102±0.062	1.724±0.203	1.049±0.071
Stem	0.336±0.029	0.248±0.022	0.149±0.022	1.549±0.082	0.970±0.028
HyperST	**0.440±0.026**	**0.368±0.026**	**0.243±0.035**	**1.267±0.059**	**0.890±0.028**

chow2). This suggests that while text supervision aids in semantic classification, it may not optimally preserve the fine-grained morphological textures essential for spatial transcriptomics prediction.

8.6. Sensitivity Analysis of Neighborhood Size K

We investigate the impact of the spatial neighborhood size K on the predictive performance of HyperST. Niche-level representations are constructed by selecting the K nearest neighbors for each target spot. In our default configuration, we set $K = 7$ (comprising the central spot and its six immediate neighbors), which naturally aligns with the 1-hop hexagonal layout of the Visium spatial transcriptomics platform.

To evaluate the model's sensitivity to the scale of spatial context, we conducted comparative experiments on the Kidney dataset by extending the neighborhood to 2-hop ($K = 19$) and 3-hop ($K = 37$) hexagonal rings. As shown in Table 12, the results indicate that larger neighborhoods lead to a performance degradation. This suggests that a localized spatial context (1-hop) provides the most relevant morphological and molecular information for spot-level gene expression inference, while excessively large neighborhoods may introduce distant biological noise, thereby supporting our default choice.

8.7. Sensitivity analysis of hyperbolic loss weight and entailment weight

To examine the robustness of our geometric components and justify the choice of hyperparameters, we conducted a grid search on the Kidney dataset regarding the hyperbolic loss weight α and the entailment weight β (Figure 9 and Figure 10). For α, we observe consistent performance gains compared to the baseline ($\alpha = 0$), followed by a broad plateau as α increases from 0.2 to 0.4. Both correlation metrics and error metrics remain stable within this region, indicating that the model is not sensitive to the exact value of α. We adopt $\alpha = 0.2$, as it achieves the lowest Mean Squared Error (MSE) while maintaining competitive correlation scores. Regarding β, the results exhibit a shallow U-shaped trend in error metrics, with a minimum at $\beta = 0.4$. This indicates that $\beta = 0.4$ provides the most effective regularization, justifying its selection for the final model.

8.8. Statistical Significance Analysis for Alignment Strategies

In the main text Section 4.3, we analyzed the impact of different alignment modules and compared HyperST with alternative alignment approaches such as MERU and CLIP. Due to the inherent high variance observed in small-scale ST datasets, we provide a detailed statistical verification here to substantiate our claims. Table 13 presents the relative performance improvement of our full HyperST model compared to the variants and baselines. The p-values are derived from paired t-tests across 5 independent experimental runs. As shown, HyperST yields statistically significant improvements ($p < 0.05$) over both the ablated variants (demonstrating the necessity of our HEA and HCA modules) and the external alignment baselines (MERU, CLIP) across the majority of metrics.

Table 9. Performance comparison on the HVG gene set of four spatial transcriptomics datasets. Higher values on PCC@10, PCC@50, PCC@200 are better. Lower values on MAE and MSE are better.

Dataset	Model	PCC@10 ↑	PCC@50 ↑	PCC@200 ↑	MSE ↓	MAE ↓
Kidney	TRIPLEX	0.541±0.094	0.453±0.087	0.331±0.068	1.138±0.255	0.843±0.098
	StNet	0.537±0.111	0.454±0.100	0.332±0.079	1.084±0.153	0.822±0.052
	BLEEP	0.508±0.123	0.426±0.114	0.306±0.087	1.181±0.219	0.853±0.080
	Stem	0.501±0.112	0.404±0.097	0.273±0.067	1.288±0.199	0.888±0.071
	HyperST	**0.618±0.099**	**0.530±0.090**	**0.399±0.071**	**1.079±0.198**	**0.821±0.082**
Colorectum	TRIPLEX	0.685±0.154	0.613±0.181	0.484±0.238	1.830±0.826	1.042±0.257
	StNet	0.656±0.122	0.578±0.138	0.447±0.181	1.642±0.427	1.009±0.154
	BLEEP	0.662±0.119	0.568±0.122	0.422±0.170	1.891±0.673	1.064±0.211
	Stem	0.679±0.111	0.574±0.124	0.415±0.173	1.799±0.613	1.045±0.205
	HyperST	**0.716±0.117**	**0.641±0.137**	**0.504±0.195**	**1.464±0.564**	**0.951±0.197**
Skin	TRIPLEX	0.826±0.093	0.795±0.112	0.745±0.136	0.957±0.488	0.675±0.219
	StNet	0.808±0.100	0.782±0.113	0.739±0.135	0.970±0.402	0.677±0.192
	BLEEP	0.782±0.108	0.755±0.120	0.708±0.139	1.117±0.559	0.696±0.224
	Stem	0.781±0.097	0.749±0.116	0.698±0.140	1.196±0.626	0.707±0.241
	HyperST	**0.838±0.089**	**0.812±0.104**	**0.766±0.127**	**0.882±0.387**	**0.631±0.181**
Lung	TRIPLEX	0.554±0.243	0.493±0.263	0.413±0.267	1.473±1.164	0.839±0.424
	StNet	0.561±0.231	0.500±0.250	0.411±0.252	1.400±1.058	0.831±0.382
	BLEEP	0.550±0.253	0.485±0.278	0.404±0.289	1.481±0.895	0.850±0.332
	Stem	0.537±0.226	0.457±0.247	0.359±0.246	1.532±1.161	0.826±0.429
	HyperST	**0.639±0.227**	**0.575±0.259**	**0.487±0.286**	**1.074±0.783**	**0.723±0.327**

Table 10. Performance of foundation encoder comparison on the Kidney dataset. Higher values on PCC@10, PCC@50, PCC@200 are better. Lower values on MAE and MSE are better.

Model	PCC@10 ↑	PCC@50 ↑	PCC@200 ↑	MSE ↓	MAE ↓
DINOv2	0.441±0.088	0.351±0.070	0.227±0.044	1.357±0.296	0.922±0.094
CONCH	0.433±0.096	0.341±0.072	0.217±0.043	1.315±0.347	0.899±0.115
Prov-GigaPath	0.501±0.096	0.405±0.085	0.267±0.056	1.270±0.163	0.897±0.083
Virchow2	0.510±0.106	0.409±0.095	0.261±0.069	1.281±0.206	0.896±0.075
UNI	0.516±0.092	0.417±0.080	0.279±0.057	1.266±0.222	0.881±0.081
HyperST	**0.617±0.094**	**0.526±0.088**	**0.390±0.070**	**1.077±0.155**	**0.817±0.058**

9. Additional Visualization

9.1. Feature Visualization

To further analyze the learned representations, we visualize the hyperbolic latent space on the Kidney dataset in Figure 11. This visualization includes (a) the distribution of Lorentz hyperbolic distances from the embeddings to the origin, and (b) a 2D projection of the image and gene latent representations. These visualization results demonstrate a clear structural ordering across groups: spot-level/image representations concentrate closer to the origin, while niche-level/gene representations tend to be farther away. This distribution is consistent with our hierarchical modeling assumption, which suggests that more information-rich biological concepts should be placed further from the origin in hyperbolic space.

9.2. Result Visualization

In this section, we present visualizations of additional marker genes across different tissues to demonstrate the robustness of our findings. We selected three samples (ZEN42, NCBI476, and MICS27) from datasets of colorectum, skin, and lung tissues, respectively, and plotted the predicted gene expressions on their H&E images for the following marker genes: COL1A1, FN1, GJB2, KRT6B, ALDH1A1, and ELF3. These genes are highly correlated with specific tissue cell types. Specifically, ALDH1A1 and ELF3 are marker genes for lung tissue [6, 10], GJB2 and KRT6B are marker genes for skin tissue [4, 9], and COL1A1 and FN1 are marker genes for Colorectum tissue [16, 20]. Visualizations of predicted gene expressions by different models, along with their PCC comparisons, are presented in Figures 12 to 17. The figures clearly demonstrate that HyperST's gene expression predictions exhibit strong consistency with the ground truth, achieving higher PCC than existing models.

Table 11. Performance comparison on four spatial transcriptomics datasets using strict patient-level splits. **Bold** indicates the best performance, and underline indicates the second-best performance.

Dataset	Model	PCC@10 ↑	PCC@50 ↑	PCC@200 ↑	MSE ↓	MAE ↓
Kidney	TRIPLEX	0.511±0.107	0.418±0.109	0.288±0.102	**1.207±0.249**	**0.868±0.100**
	StNet	0.503±0.079	0.425±0.079	0.303±0.077	1.332±0.311	0.917±0.166
	BLEEP	0.495±0.083	0.407±0.085	0.279±0.086	1.368±0.365	0.915±0.137
	Stem	0.468±0.073	0.365±0.063	0.227±0.059	1.449±0.323	0.942±0.115
	HyperST	**0.587±0.065**	**0.495±0.069**	**0.357±0.074**	1.283±0.362	0.889±0.140
Colorectum	TRIPLEX	0.685±0.115	0.613±0.128	0.418±0.116	2.423±0.744	1.187±0.187
	StNet	0.654±0.111	0.585±0.114	0.386±0.091	2.284±0.319	1.155±0.098
	BLEEP	0.612±0.119	0.538±0.117	0.340±0.081	2.551±0.513	1.213±0.137
	Stem	0.653±0.136	0.560±0.126	0.357±0.086	2.351±0.504	1.166±0.144
	HyperST	**0.712±0.096**	**0.642±0.093**	**0.448±0.078**	**2.152±0.515**	**1.131±0.152**
Skin	TRIPLEX	0.816±0.089	0.783±0.108	0.726±0.131	1.361±0.701	0.812±0.196
	StNet	0.786±0.102	0.759±0.112	0.704±0.128	1.407±0.652	0.832±0.194
	BLEEP	0.789±0.102	0.761±0.116	0.705±0.132	1.479±0.627	0.826±0.204
	Stem	0.765±0.103	0.734±0.117	0.673±0.132	1.743±1.040	0.898±0.264
	HyperST	**0.828±0.079**	**0.799±0.093**	**0.746±0.111**	**1.310±0.727**	**0.792±0.210**
Lung	TRIPLEX	0.415±0.171	0.324±0.180	0.207±0.161	1.727±1.467	0.884±0.402
	StNet	0.414±0.182	0.330±0.190	0.224±0.173	1.593±1.140	0.878±0.331
	BLEEP	0.346±0.144	0.258±0.152	0.158±0.149	1.832±1.367	0.886±0.396
	Stem	0.386±0.147	0.288±0.161	0.181±0.147	1.587±1.326	**0.826±0.377**
	HyperST	**0.491±0.203**	**0.388±0.225**	**0.260±0.222**	**1.482±0.950**	0.843±0.304

Table 12. Sensitivity study of K for KNN-based niche definition. **Bold** indicates the best performance.

K	PCC@10 ↑	PCC@50 ↑	PCC@200 ↑	MSE ↓	MAE ↓
7	**0.617**	**0.526**	**0.390**	**1.077**	**0.817**
19	0.602	0.512	0.379	1.092	0.823
37	0.602	0.504	0.368	1.113	0.830

Table 13. Statistical significance analysis for Alignment Strategies on the Kidney datasets. We report the **relative improvement** of HyperST over each variant and the corresponding p**-value** (in parentheses) from a paired t-test. Values with $p < 0.05$ indicate statistically significant improvements.

Alignment	PCC@10 ↑	PCC@50 ↑	PCC@200 ↑	MSE ↓	MAE ↓
w/o G-I HEA	2.21% (< 0.05)	2.18% (< 0.05)	3.24% (< 0.05)	6.06% (< 0.05)	2.58% (0.055)
w/o HEA	2.34% (< 0.05)	3.52% (< 0.05)	6.01% (< 0.05)	3.63% (< 0.05)	1.65% (< 0.05)
w/o HEA + HCA	7.21% (< 0.05)	8.58% (< 0.05)	13.26% (< 0.05)	5.01% (< 0.05)	2.36% (< 0.05)
MERU	5.40% (< 0.05)	6.46% (< 0.05)	9.87% (< 0.05)	6.12% (< 0.05)	3.01% (< 0.05)
CLIP	10.62% (< 0.05)	13.75% (< 0.05)	21.61% (< 0.05)	11.68% (< 0.05)	5.76% (< 0.05)

Dataset	Genes to be predicted
Kidney	'A2M', 'ACADVL', 'ACTA2', 'ACTB', 'ACTG1', 'ADGRG1', 'ADIRF', 'AEBP1', 'ALDOB', 'ANPEP', 'ANXA2', 'APLP2', 'APOE', 'APP', 'AQP1', 'AQP2', 'ASAH1', 'ASS1', 'ATP1A1', 'ATP1B1', 'ATP5F1A', 'ATP5F1D', 'ATP5MC3', 'ATP5ME', 'ATP5MF', 'ATP6V0C', 'B2M', 'BCAM', 'BGN', 'BSG', 'C1QA', 'C1R', 'C7', 'CA2', 'CALB1', 'CALD1', 'CALM1', 'CALM2', 'CANX', 'CD151', 'CD24', 'CD74', 'CD81', 'CD9', 'CDH16', 'CDKN1C', 'CFL1', 'CHCHD10', 'CHCHD2', 'CIRBP', 'CKB', 'CLCNKB', 'CLU', 'COL1A2', 'COL3A1', 'COL4A1', 'COL4A2', 'COX5A', 'COX5B', 'COX6A1', 'COX6B1', 'COX6C', 'COX7A2', 'COX7B', 'COX7C', 'COX8A', 'CRIM1', 'CRYAB', 'CST3', 'CTSB', 'CTSH', 'CXCL12', 'CXCL14', 'CYSTM1', 'DCN', 'DDX17', 'DDX5', 'DEFB1', 'DSTN', 'DUSP1', 'DYNLL1', 'EEF1A1', 'EEF1D', 'EEF1G', 'EEF2', 'EFHD1', 'EIF3K', 'EIF4A1', 'ENG', 'EPAS1', 'EZR', 'FABP1', 'FAU', 'FLNA', 'FTH1', 'FTL', 'FXYD2', 'FXYD4', 'GABARAP', 'GATM', 'GHITM', 'GPX3', 'GSTM3', 'GSTP1', 'GTF2I', 'HINT1', 'HLA-A', 'HLA-B', 'HLA-C', 'HLA-DPA1', 'HLA-DRA', 'HLA-DRB1', 'HLA-E', 'HNRNPA1', 'HNRNPA2B1', 'HSD11B2', 'HSP90AB1', 'HSPA8', 'HSPB1', 'HTRA1', 'IDH2', 'IFITM2', 'IFITM3', 'IGFBP2', 'IGFBP4', 'IGFBP5', 'IGFBP7', 'IGHA1', 'IGHG1', 'IGHG3', 'IGHG4', 'IGKC', 'IGLC1', 'IGLC2', 'IGLC3', 'ITGA3', 'ITGB1', 'ITM2B', 'IVNS1ABP', 'KCNJ1', 'KCNJ15', 'KNG1', 'LAMP1', 'LAMTOR5', 'LAPTM4A', 'LDHA', 'LGALS1', 'LRP2', 'LUM', 'MAL', 'MALAT1', 'MGP', 'MGST1', 'MGST3', 'MIF', 'MIOX', 'MMP7', 'MUC1', 'MYL12A', 'MYL6', 'MYL9', 'MZT2B', 'NAT8', 'NDRG1', 'NDUFA1', 'NDUFA13', 'NDUFA2', 'NDUFA4', 'NDUFA6', 'NDUFB2', 'NDUFB7', 'NDUFB8', 'NDUFB9', 'NDUFC1', 'NDUFS5', 'NDUFS6', 'NDUFV1', 'NEAT1', 'NME2', 'NPC2', 'OAZ1', 'OGDHL', 'OST4', 'P4HB', 'PCBP1', 'PCK1', 'PDZK1IP1', 'PEBP1', 'PEPD', 'PFN1', 'PGK1', 'PHPT1', 'PIGR', 'PODXL', 'POLR2L', 'PPP1R1A', 'PTGDS', 'PTH1R', 'REN', 'RHCG', 'RHOA', 'RNASE1', 'ROMO1', 'RTN4', 'S100A10', 'S100A2', 'S100A6', 'SAT1', 'SDC1', 'SELENOP', 'SERPINA1', 'SERPINA5', 'SFRP1', 'SLC12A1', 'SLC12A3', 'SLC13A3', 'SLC25A3', 'SLC25A5', 'SLC25A6', 'SLC3A1', 'SLC5A12', 'SMIM24', 'SNHG25', 'SOD1', 'SOD2', 'SPARC', 'SPINK1', 'SPP1', 'SRP14', 'SSR4', 'SUCLG1', 'TAGLN', 'TAGLN2', 'THY1', 'TIMP1', 'TIMP2', 'TIMP3', 'TINAGL1', 'TMA7', 'TMSB10', 'TMSB4X', 'TPI1', 'TPM1', 'TPT1', 'TSPAN1', 'TUBB', 'TXN', 'UBA52', 'UGT2B7', 'UMOD', 'UQCRB', 'UQCRC1', 'UQCRFS1', 'VIM', 'WFDC2'
Colorectum	'A2M', 'ACTA2', 'AEBP1', 'AGR2', 'AHNAK', 'ANXA11', 'APOE', 'ASS1', 'ATP1B1', 'ATP5ME', 'ATP6V0C', 'B2M', 'BCAP31', 'BGN', 'BST2', 'BTF3', 'C15orf48', 'C19orf33', 'C1QA', 'C1QB', 'C1R', 'C1S', 'C3', 'CALD1', 'CALM1', 'CCN2', 'CD24', 'CD44', 'CD55', 'CD59', 'CD74', 'CD81', 'CD99', 'CDH17', 'CEACAM5', 'CEACAM6', 'CEACAM7', 'CKB', 'CLCA1', 'CLDN3', 'CLDN4', 'CLDN7', 'COL12A1', 'COL18A1', 'COL1A1', 'COL1A2', 'COL3A1', 'COL4A1', 'COL4A2', 'COL5A1', 'COL5A2', 'COL6A1', 'COL6A2', 'COL6A3', 'COMMD6', 'COX5A', 'COX5B', 'COX6B1', 'COX7B', 'CRIP1', 'CSTB', 'CTSB', 'CTSC', 'CTSD', 'CXCL1', 'CXCL10', 'CXCL14', 'DBI', 'DCN', 'DEFA5', 'DMBT1', 'DUOX2', 'DUSP1', 'EEF1A1', 'EGR1', 'EIF5A', 'ELF3', 'ENO1', 'EPCAM', 'FABP1', 'FAM3D', 'FBLN1', 'FCGBP', 'FLNA', 'FN1', 'FOS', 'FSTL1', 'FTH1', 'FTL', 'FXYD3', 'GPRC5A', 'GPX2', 'GREM1', 'GSN', 'HLA-A', 'HLA-B', 'HLA-C', 'HLA-DPA1', 'HLA-DPB1', 'HLA-DQB1', 'HLA-DRA', 'HLA-DRB1', 'HMGN2', 'HNRNPH1', 'HNRNPU', 'HSPB1', 'HSPD1', 'ID1', 'IDO1', 'IER2', 'IER3', 'IFI30', 'IFI6', 'IGFBP4', 'IGFBP5', 'IGFBP7', 'IGHA1', 'IGHG1', 'IGHG3', 'IGHG4', 'IGHM', 'IGKC', 'IGLC1', 'IGLC2', 'IGLC3', 'IL32', 'IRF1', 'ISG15', 'ITLN1', 'ITM2B', 'ITM2C', 'JCHAIN', 'JUNB', 'JUND', 'JUP', 'KDELR2', 'KLF5', 'KRT18', 'KRT19', 'KRT8', 'LCN2', 'LDHB', 'LGALS1', 'LGALS3', 'LGALS4', 'LUM', 'LY6E', 'LYZ', 'MALAT1', 'MARCKSL1', 'MDK', 'MGP', 'MMP1', 'MMP11', 'MMP2', 'MUC1', 'MUC12', 'MUC13', 'MUC2', 'MUC5B', 'MYL12B', 'MYL9', 'NBL1', 'NDUFA13', 'NORAD', 'NR4A1', 'OLFM4', 'PABPC1', 'PERP', 'PGK1', 'PHGR1', 'PI3', 'PIGR', 'PLA2G2A', 'POSTN', 'PPIB', 'PRSS8', 'PSMB8', 'PTMA', 'RBM3', 'REG1A', 'REG3A', 'REG4', 'RHOA', 'RHOC', 'ROMO1', 'RRBP1', 'S100A14', 'S100A6', 'S100A8', 'S100A9', 'S100P', 'SAT1', 'SELENOP', 'SERPINA1', 'SERPING1', 'SFN', 'SLC12A2', 'SMIM22', 'SNRPB', 'SOD2', 'SPARC', 'SPINK1', 'SPINK4', 'SPINT2', 'SPTBN1', 'ST14', 'STAT1', 'SULF1', 'TAGLN', 'TFF1', 'TFF3', 'TGFBI', 'THBS1', 'THY1', 'TIMP1', 'TIMP2', 'TM9SF2', 'TMEM176B', 'TMEM54', 'TMEM59', 'TMSB4X', 'TPM2', 'TPT1', 'TSPAN1', 'TSPAN3', 'TSPAN8', 'TSPO', 'TYMP', 'UBD', 'UQCR11', 'UQCRH', 'VIM', 'YWHAB', 'ZFP36', 'ZG16'

Figure 5. HMHVG gene selection in Kidney and Colorectum

Dataset	Genes to be predicted
Skin	'ACTB', 'ACTG1', 'AHNAK', 'ANXA1', 'ANXA2', 'APRT', 'AQP3', 'ARPC2', 'ASPRV1', 'ATP1B3', 'ATP5F1A', 'ATP5F1B', 'ATP5F1E', 'ATP5MC2', 'ATP5MC3', 'ATP5ME', 'ATP5MF', 'ATP5MG', 'B2M', 'BTF3', 'C19orf33', 'CALM1', 'CALML3', 'CALML5', 'CASP14', 'CCL27', 'CD24', 'CD44', 'CD74', 'CD9', 'CDSN', 'CFL1', 'CHCHD2', 'CLTB', 'CNBP', 'CNFN', 'COL17A1', 'COL1A1', 'COL1A2', 'COL3A1', 'COL6A1', 'COL6A2', 'COX4I1', 'COX5B', 'COX6A1', 'COX6B1', 'COX6C', 'COX7A2', 'COX7B', 'COX7C', 'COX8A', 'CRABP2', 'CSNK1A1', 'CST3', 'CST6', 'CSTA', 'CSTB', 'CTNNBIP1', 'CTSB', 'CTSD', 'CXCL14', 'DBI', 'DCD', 'DCN', 'DEFB4A', 'DEGS1', 'DMKN', 'DSC1', 'DSC3', 'DSG1', 'DSG3', 'DSP', 'DSTN', 'DYNLL1', 'EEF1A1', 'EEF1B2', 'EEF1D', 'EEF2', 'EIF1', 'EIF3E', 'EIF3F', 'EIF4G2', 'EIF5A', 'ELOB', 'ENO1', 'FABP5', 'FADS2', 'FAM25A', 'FAU', 'FLG', 'FLG2', 'FTH1', 'FTL', 'GAPDH', 'GJA1', 'GJB2', 'GLTP', 'GPNMB', 'GSTP1', 'GUK1', 'H3-3A', 'H3-3B', 'HINT1', 'HLA-B', 'HLA-C', 'HLA-DPA1', 'HLA-DPB1', 'HLA-DQB1', 'HLA-DRA', 'HLA-DRB1', 'HLA-E', 'HMGB1', 'HNRNPA1', 'HNRNPA2B1', 'HNRNPK', 'HOPX', 'HSP90AA1', 'HSP90AB1', 'HSPA8', 'HSPB1', 'IFI27', 'IFI6', 'IFITM3', 'IGKC', 'ITM2B', 'IVL', 'KLF5', 'KLK7', 'KRT1', 'KRT10', 'KRT14', 'KRT16', 'KRT17', 'KRT2', 'KRT5', 'KRT6A', 'KRT6B', 'KRT6C', 'KRTDAP', 'LAD1', 'LCE1B', 'LCE3D', 'LDHA', 'LGALS1', 'LGALS3', 'LGALS7', 'LGALS7B', 'LMNA', 'LY6D', 'LYPD3', 'LYZ', 'MIF', 'MUCL1', 'MYL6', 'NACA', 'NCCRP1', 'NDUFA4', 'NDUFS5', 'NOP53', 'NPM1', 'OAZ1', 'P4HB', 'PABPC1', 'PERP', 'PFDN5', 'PFN1', 'PGAM1', 'PI3', 'PKM', 'PKP1', 'PLP2', 'POLR2L', 'PPDPF', 'PPIA', 'PPL', 'PRDX1', 'PSAP', 'PSMA7', 'PTMA', 'RAB11A', 'RAC1', 'RACK1', 'RAN', 'RBM3', 'ROMO1', 'RTN4', 'S100A10', 'S100A11', 'S100A14', 'S100A16', 'S100A2', 'S100A4', 'S100A6', 'S100A7', 'S100A8', 'S100A9', 'SBSN', 'SCGB2A2', 'SDC1', 'SELENOW', 'SERBP1', 'SERF2', 'SERPINB3', 'SERPINB4', 'SERPINB5', 'SFN', 'SH3BGRL3', 'SLC25A3', 'SLC25A5', 'SLC25A6', 'SLC2A1', 'SLPI', 'SLURP1', 'SNRPD2', 'SPARC', 'SPINK5', 'SPINT2', 'SPRR1B', 'SPRR2A', 'SPRR2B', 'SPRR2D', 'SPRR2E', 'SPRR2G', 'SUB1', 'TACSTD2', 'TAGLN2', 'TMA7', 'TMBIM6', 'TMEM45A', 'TMSB10', 'TMSB4X', 'TOMM7', 'TPI1', 'TPT1', 'TRIM29', 'TSPO', 'TUBA1B', 'TUBA1C', 'TUBB4B', 'TXN', 'TYMP', 'UBA52', 'UBB', 'UBC', 'UBL5', 'UQCR10', 'UQCR11', 'UQCRB', 'UQCRQ', 'VIM', 'YBX1', 'YBX3', 'YWHAB', 'YWHAZ'
Lung	'A2M', 'ACTA2', 'ACTG1', 'ACTG2', 'ADIRF', 'AEBP1', 'AGR2', 'AHNAK', 'ALDH1A1', 'ANXA1', 'ANXA2', 'APLP2', 'APOD', 'AQP1', 'AQP3', 'ARF1', 'ATP5F1A', 'ATP5F1B', 'ATP5IF1', 'ATP5MC2', 'ATP5ME', 'ATP5MG', 'AZGP1', 'B2M', 'BGN', 'BPIFA1', 'BPIFB1', 'BPIFB2', 'C11orf96', 'C1QA', 'C3', 'C9orf24', 'CALM1', 'CALM2', 'CALR', 'CANX', 'CAPS', 'CD151', 'CD24', 'CD59', 'CD63', 'CD81', 'CD9', 'CDC42', 'CFD', 'CHCHD2', 'CIB1', 'CKB', 'CLU', 'COL1A1', 'COL1A2', 'COL3A1', 'COL6A2', 'COX5B', 'COX6A1', 'COX6B1', 'COX6C', 'COX7A2', 'COX7C', 'COX8A', 'CSRP1', 'CST3', 'CSTB', 'CTNNA1', 'CTSB', 'CTSC', 'CTSD', 'CXCL17', 'DCN', 'DDIT4', 'DDX5', 'DES', 'DHCR24', 'DMBT1', 'DUSP1', 'DYNLL1', 'EEF1A1', 'EEF1D', 'EIF1', 'ELF3', 'ELOB', 'EPAS1', 'EZR', 'FBLN1', 'FCGBP', 'FLNA', 'FN1', 'FOS', 'FTH1', 'FTL', 'FXYD3', 'GAPDH', 'GLUL', 'GPX3', 'GPX4', 'GSTP1', 'HBA1', 'HBA2', 'HINT1', 'HLA-B', 'HLA-C', 'HLA-DRA', 'HLA-DRB1', 'HLA-E', 'HMGN2', 'HNRNPA2B1', 'HNRNPK', 'HSBP1', 'HSPA1A', 'HSPA8', 'HSPB1', 'IFITM2', 'IFITM3', 'IGFBP4', 'IGFBP7', 'IGHA1', 'IGHG1', 'IGHG3', 'IGHM', 'IGKC', 'IGLC2', 'IGLC3', 'ITM2B', 'JCHAIN', 'KRT15', 'KRT17', 'KRT19', 'KRT7', 'LAPTM4A', 'LCN2', 'LGALS1', 'LGALS3', 'LTF', 'LYZ', 'MALAT1', 'MFGE8', 'MGP', 'MORF4L1', 'MSMB', 'MUC1', 'MUC4', 'MUC5AC', 'MUC5B', 'MYH11', 'MYL12B', 'MYL9', 'NACA', 'NAPSA', 'NDUFA4', 'NDUFB1', 'NEAT1', 'NOP53', 'NPC2', 'NPM1', 'NUPR1', 'P4HB', 'PABPC1', 'PCBP2', 'PERP', 'PGC', 'PIP', 'PKM', 'PLA2G2A', 'PLXNB2', 'PPDPF', 'PPP1CB', 'PRB3', 'PRB4', 'PRDX1', 'PRH2', 'PRKAR1A', 'PRR4', 'PRSS23', 'PSAP', 'PTMA', 'RHOA', 'RHOB', 'RNASE1', 'RSPH1', 'S100A10', 'S100A11', 'S100A2', 'S100A9', 'S100P', 'SAA1', 'SAA2', 'SAT1', 'SCGB1A1', 'SCGB3A1', 'SDC4', 'SERF2', 'SERPINA1', 'SERPINB3', 'SFTPA1', 'SFTPA2', 'SFTPB', 'SFTPC', 'SH3BGRL3', 'SKP1', 'SLC34A2', 'SLC44A4', 'SLPI', 'SMIM22', 'SNHG25', 'SOD1', 'SPARC', 'SPARCL1', 'SRP14', 'SSR4', 'STOM', 'TACSTD2', 'TAGLN', 'TAGLN2', 'TFF3', 'TGM2', 'TIMP1', 'TIMP3', 'TMA7', 'TMEM59', 'TMSB4X', 'TPI1', 'TPM2', 'TPPP3', 'TPT1', 'TSC22D1', 'TSPAN1', 'TSPAN3', 'TSPO', 'TUBA1A', 'TUBA1B', 'TUBB', 'TUBB4B', 'TXN', 'UBB', 'UBC', 'UBL5', 'UQCR11', 'UQCRQ', 'VAMP8', 'VIM', 'VWF', 'WFDC2', 'YWHAE', 'ZFP36', 'ZFP36L1', 'ZG16B'

Figure 6. HMHVG gene selection in Skin and Lung

Dataset	Genes to be predicted
Kidney	'A2M', 'ACADVL', 'ACAT1', 'ACO2', 'ACTA2', 'ACTB', 'ACTG1', 'ADGRG1', 'ADI1', 'ADIRF', 'AEBP1', 'ALDOB', 'ANAPC16', 'ANPEP', 'ANXA2', 'ANXA5', 'APLP2', 'APOE', 'APP', 'AQP1', 'AQP2', 'ARHGDIA', 'ASAH1', 'ASS1', 'ATP1A1', 'ATP1B1', 'ATP5F1A', 'ATP5F1D', 'ATP5MC3', 'ATP5ME', 'ATP5MF', 'ATP6AP2', 'ATP6V0C', 'ATP6V1F', 'B2M', 'BCAM', 'BGN', 'BSG', 'C1QA', 'C1R', 'C7', 'CA2', 'CALB1', 'CALD1', 'CALM1', 'CALM2', 'CANX', 'CAPN2', 'CD151', 'CD24', 'CD74', 'CD81', 'CD9', 'CDH16', 'CDKN1C', 'CFL1', 'CHCHD10', 'CHCHD2', 'CIRBP', 'CKB', 'CLCNKB', 'CLTC', 'CLU', 'COL1A2', 'COL3A1', 'COL4A1', 'COL4A2', 'COX5A', 'COX5B', 'COX6A1', 'COX6B1', 'COX6C', 'COX7A2', 'COX7B', 'COX7C', 'COX8A', 'CRIM1', 'CRIP2', 'CRYAB', 'CSDE1', 'CSRP1', 'CST3', 'CTSB', 'CTSH', 'CXCL12', 'CXCL14', 'CYSTM1', 'DCN', 'DDT', 'DDX17', 'DDX5', 'DEFB1', 'DSTN', 'DUSP1', 'DYNLL1', 'DYNLL2', 'EEF1A1', 'EEF1D', 'EEF1G', 'EEF2', 'EFHD1', 'EIF3K', 'EIF4A1', 'EIF4A2', 'EIF4B', 'ENG', 'EPAS1', 'EZR', 'FABP1', 'FAU', 'FCGRT', 'FLNA', 'FTH1', 'FTL', 'FXYD2', 'FXYD4', 'GABARAP', 'GATM', 'GHITM', 'GPX3', 'GSN', 'GSTM3', 'GSTP1', 'GTF2I', 'HINT1', 'HLA-A', 'HLA-B', 'HLA-C', 'HLA-DPA1', 'HLA-DRA', 'HLA-DRB1', 'HLA-E', 'HNRNPA1', 'HNRNPA2B1', 'HNRNPH1', 'HSD11B2', 'HSP90AB1', 'HSPA8', 'HSPB1', 'HSPD1', 'HTRA1', 'IDH2', 'IFITM2', 'IFITM3', 'IGFBP2', 'IGFBP4', 'IGFBP5', 'IGFBP7', 'IGHA1', 'IGHG1', 'IGHG3', 'IGHG4', 'IGKC', 'IGLC1', 'IGLC2', 'IGLC3', 'ITGA3', 'ITGB1', 'ITM2B', 'IVNS1ABP', 'JUND', 'KCNJ1', 'KCNJ15', 'KNG1', 'LAMB2', 'LAMP1', 'LAMTOR5', 'LAPTM4A', 'LDHA', 'LGALS1', 'LITAF', 'LRP2', 'LUM', 'MAL', 'MALAT1', 'METTL7A', 'MGP', 'MGST1', 'MGST3', 'MIF', 'MIOX', 'MMP7', 'MUC1', 'MYL12A', 'MYL6', 'MYL9', 'MZT2B', 'NAT8', 'NDRG1', 'NDUFA1', 'NDUFA13', 'NDUFA2', 'NDUFA4', 'NDUFA6', 'NDUFB2', 'NDUFB7', 'NDUFB8', 'NDUFB9', 'NDUFC1', 'NDUFS5', 'NDUFS6', 'NDUFV1', 'NEAT1', 'NME2', 'NOP53', 'NORAD', 'NPC2', 'NUCB1', 'OAZ1', 'OGDHL', 'OST4', 'P4HB', 'PCBP1', 'PCK1', 'PDZK1IP1', 'PEBP1', 'PEPD', 'PFKL', 'PFN1', 'PGAM1', 'PGK1', 'PHPT1', 'PIGR', 'PODXL', 'POLR2L', 'PPIB', 'PPP1R1A', 'PTGDS', 'PTH1R', 'RABAC1', 'RAC1', 'REN', 'RHCG', 'RHOA', 'RNASE1', 'ROMO1', 'RTN4', 'S100A10', 'S100A2', 'S100A6', 'SAT1', 'SCNN1A', 'SCP2', 'SDC1', 'SELENOM', 'SELENOP', 'SERPINA1', 'SERPINA5', 'SFRP1', 'SH3BGRL3', 'SLC12A1', 'SLC12A3', 'SLC13A3', 'SLC25A3', 'SLC25A5', 'SLC25A6', 'SLC3A1', 'SLC5A12', 'SMIM24', 'SNHG25', 'SOD1', 'SOD2', 'SPARC', 'SPINK1', 'SPP1', 'SRP14', 'SSR4', 'ST13', 'SUCLG1', 'SUMO2', 'TAGLN', 'TAGLN2', 'TAPBP', 'THY1', 'TIMP1', 'TIMP2', 'TIMP3', 'TINAGL1', 'TMA7', 'TMSB10', 'TMSB4X', 'TPI1', 'TPM1', 'TPM3', 'TPT1', 'TRIR', 'TSC22D1', 'TSPAN1', 'TUBA1A', 'TUBB', 'TXN', 'UBA52', 'UGT2B7', 'UMOD', 'UQCRB', 'UQCRC1', 'UQCRFS1', 'VIM', 'WFDC2', 'ZFP36L2'
Colorectum	'A2M', 'ACTA2', 'AEBP1', 'AGR2', 'AHNAK', 'ANXA11', 'ANXA5', 'APLP2', 'APOE', 'ARPC2', 'ASS1', 'ATP1B1', 'ATP5F1A', 'ATP5IF1', 'ATP5ME', 'ATP6V0B', 'ATP6V0C', 'B2M', 'BCAP31', 'BGN', 'BST2', 'BTF3', 'C15orf48', 'C19orf33', 'C1QA', 'C1QB', 'C1R', 'C1S', 'C3', 'CALD1', 'CALM1', 'CALM3', 'CAPZB', 'CCN2', 'CCND1', 'CD24', 'CD44', 'CD55', 'CD59', 'CD74', 'CD81', 'CD99', 'CDH17', 'CEACAM5', 'CEACAM6', 'CEACAM7', 'CHCHD10', 'CIRBP', 'CKB', 'CLCA1', 'CLDN3', 'CLDN4', 'CLDN7', 'CLTA', 'COL12A1', 'COL18A1', 'COL1A1', 'COL1A2', 'COL3A1', 'COL4A1', 'COL4A2', 'COL5A1', 'COL5A2', 'COL6A1', 'COL6A2', 'COL6A3', 'COMMD6', 'COX5A', 'COX5B', 'COX6B1', 'COX7B', 'CRIP1', 'CSTB', 'CTSB', 'CTSC', 'CTSD', 'CTSS', 'CXCL1', 'CXCL10', 'CXCL14', 'CYCS', 'DBI', 'DCN', 'DEFA5', 'DMBT1', 'DUOX2', 'DUSP1', 'EEF1A1', 'EGR1', 'EIF3K', 'EIF5A', 'ELF3', 'ENO1', 'EPCAM', 'FABP1', 'FAM3D', 'FBLN1', 'FCGBP', 'FLNA', 'FN1', 'FOS', 'FSTL1', 'FTH1', 'FTL', 'FXYD3', 'GAS5', 'GLUL', 'GNB1', 'GPI', 'GPRC5A', 'GPX2', 'GREM1', 'GSN', 'HLA-A', 'HLA-B', 'HLA-C', 'HLA-DPA1', 'HLA-DPB1', 'HLA-DQB1', 'HLA-DRA', 'HLA-DRB1', 'HMGN1', 'HMGN2', 'HNRNPAB', 'HNRNPH1', 'HNRNPU', 'HSPB1', 'HSPD1', 'HSPG2', 'ID1', 'IDO1', 'IER2', 'IER3', 'IFI30', 'IFI6', 'IGFBP4', 'IGFBP5', 'IGFBP7', 'IGHA1', 'IGHG1', 'IGHG3', 'IGHG4', 'IGHM', 'IGKC', 'IGLC1', 'IGLC2', 'IGLC3', 'IL32', 'IRF1', 'ISG15', 'ITLN1', 'ITM2B', 'ITM2C', 'JCHAIN', 'JTB', 'JUNB', 'JUND', 'JUP', 'KDELR2', 'KLF5', 'KRT18', 'KRT19', 'KRT8', 'KRTCAP2', 'LCN2', 'LDHB', 'LGALS1', 'LGALS3', 'LGALS4', 'LUM', 'LY6E', 'LYZ', 'MALAT1', 'MARCKSL1', 'MDK', 'MGP', 'MGST1', 'MLEC', 'MMP1', 'MMP11', 'MMP2', 'MORF4L2', 'MUC1', 'MUC12', 'MUC13', 'MUC2', 'MUC5B', 'MYL12B', 'MYL9', 'NAMPT', 'NBL1', 'NDUFA13', 'NDUFB1', 'NDUFS6', 'NOP53', 'NORAD', 'NR4A1', 'OLFM4', 'PABPC1', 'PDIA4', 'PERP', 'PFKL', 'PGK1', 'PHGR1', 'PI3', 'PIGR', 'PLA2G2A', 'POLR2L', 'POSTN', 'PPIB', 'PRDX2', 'PRDX6', 'PRR13', 'PRSS8', 'PSMA1', 'PSMA4', 'PSMB8', 'PTBP1', 'PTGES3', 'PTMA', 'PTMS', 'QSOX1', 'RAB1A', 'RBM3', 'REG1A', 'REG3A', 'REG4', 'RHOA', 'RHOB', 'RHOC', 'RNASE1', 'RNASEK', 'ROMO1', 'RRBP1', 'S100A14', 'S100A4', 'S100A6', 'S100A8', 'S100A9', 'S100P', 'SAT1', 'SDC4', 'SEC61A1', 'SELENOP', 'SELENOW', 'SERBP1', 'SERPINA1', 'SERPING1', 'SFN', 'SKP1', 'SLC12A2', 'SMIM22', 'SNRPB', 'SOD2', 'SPARC', 'SPINK1', 'SPINK4', 'SPINT2', 'SPTBN1', 'SRP14', 'SRRM2', 'SRSF3', 'SSR3', 'ST14', 'STAT1', 'SULF1', 'TAGLN', 'TFF1', 'TFF3', 'TGFBI', 'THBS1', 'THY1', 'TIMP1', 'TIMP2', 'TM9SF2', 'TMED10', 'TMEM176B', 'TMEM54', 'TMEM59', 'TMSB4X', 'TPM2', 'TPT1', 'TSPAN1', 'TSPAN3', 'TSPAN8', 'TSPO', 'TST', 'TXNDC5', 'TYMP', 'UBD', 'UQCR10', 'UQCR11', 'UQCRH', 'VIM', 'XBP1', 'YWHAB', 'ZFAS1', 'ZFP36', 'ZFP36L1', 'ZG16'

Figure 7. HVG gene selection in Kidney and Colorectum

Dataset	Genes to be predicted
Skin	'ACTB', 'ACTG1', 'ACTN4', 'AHNAK', 'AHNAK2', 'ANXA1', 'ANXA2', 'APOE', 'APRT', 'AQP3', 'ARPC2', 'ASPRV1', 'ATP1B3', 'ATP5F1A', 'ATP5F1B', 'ATP5F1E', 'ATP5MC2', 'ATP5MC3', 'ATP5ME', 'ATP5MF', 'ATP5MG', 'ATP5PD', 'B2M', 'BTF3', 'BTG1', 'C19orf33', 'C4orf3', 'CALM1', 'CALM2', 'CALML3', 'CALML5', 'CASP14', 'CCL27', 'CD24', 'CD44', 'CD63', 'CD74', 'CD81', 'CD9', 'CDSN', 'CFL1', 'CHCHD2', 'CLTB', 'CNBP', 'CNFN', 'COL17A1', 'COL1A1', 'COL1A2', 'COL3A1', 'COL6A1', 'COL6A2', 'COX4I1', 'COX5B', 'COX6A1', 'COX6B1', 'COX6C', 'COX7A2', 'COX7B', 'COX7C', 'COX8A', 'CRABP2', 'CSDE1', 'CSNK1A1', 'CST3', 'CST6', 'CSTA', 'CSTB', 'CTNNBIP1', 'CTSB', 'CTSD', 'CXCL14', 'DBI', 'DCD', 'DCN', 'DDX5', 'DEFB4A', 'DEGS1', 'DMKN', 'DSC1', 'DSC3', 'DSG1', 'DSG3', 'DSP', 'DSTN', 'DYNLL1', 'EEF1A1', 'EEF1B2', 'EEF1D', 'EEF2', 'EIF1', 'EIF3E', 'EIF3F', 'EIF3K', 'EIF4G2', 'EIF5A', 'ELOB', 'EMP2', 'ENO1', 'EZR', 'FABP5', 'FADS2', 'FAM25A', 'FAU', 'FLG', 'FLG2', 'FTH1', 'FTL', 'GAPDH', 'GJA1', 'GJB2', 'GLTP', 'GPNMB', 'GPX4', 'GRN', 'GSN', 'GSTP1', 'GUK1', 'H3-3A', 'H3-3B', 'HINT1', 'HLA-B', 'HLA-C', 'HLA-DPA1', 'HLA-DPB1', 'HLA-DQB1', 'HLA-DRA', 'HLA-DRB1', 'HLA-E', 'HMGB1', 'HMGN2', 'HNRNPA1', 'HNRNPA2B1', 'HNRNPK', 'HOPX', 'HSP90AA1', 'HSP90AB1', 'HSP90B1', 'HSPA8', 'HSPB1', 'IFI27', 'IFI6', 'IFITM3', 'IGFBP7', 'IGKC', 'ITM2B', 'IVL', 'KLF4', 'KLF5', 'KLK7', 'KRT1', 'KRT10', 'KRT14', 'KRT16', 'KRT17', 'KRT2', 'KRT5', 'KRT6A', 'KRT6B', 'KRT6C', 'KRTDAP', 'LAD1', 'LAPTM4A', 'LCE1B', 'LCE3D', 'LDHA', 'LGALS1', 'LGALS3', 'LGALS7', 'LGALS7B', 'LMNA', 'LY6D', 'LYPD3', 'LYZ', 'MIF', 'MUCL1', 'MYL12A', 'MYL6', 'MZT2B', 'NACA', 'NAP1L1', 'NCCRP1', 'NDUFA1', 'NDUFA4', 'NDUFB1', 'NDUFB4', 'NDUFC1', 'NDUFS5', 'NOP53', 'NPM1', 'OAZ1', 'OST4', 'P4HB', 'PABPC1', 'PCBP1', 'PCBP2', 'PERP', 'PFDN5', 'PFN1', 'PGAM1', 'PGK1', 'PI3', 'PKM', 'PKP1', 'PLP2', 'POLR2L', 'PPDPF', 'PPIA', 'PPIB', 'PPL', 'PPP1R14B', 'PRDX1', 'PSAP', 'PSMA7', 'PTMA', 'RAB11A', 'RAC1', 'RACK1', 'RAN', 'RBM3', 'RHOA', 'ROMO1', 'RTN4', 'S100A10', 'S100A11', 'S100A14', 'S100A16', 'S100A2', 'S100A4', 'S100A6', 'S100A7', 'S100A8', 'S100A9', 'SBSN', 'SCGB2A2', 'SDC1', 'SELENOW', 'SEM1', 'SERBP1', 'SERF2', 'SERPINB3', 'SERPINB4', 'SERPINB5', 'SFN', 'SH3BGRL3', 'SKP1', 'SLC25A3', 'SLC25A5', 'SLC25A6', 'SLC2A1', 'SLC38A2', 'SLPI', 'SLURP1', 'SNRPD2', 'SPARC', 'SPINK5', 'SPINT2', 'SPRR1B', 'SPRR2A', 'SPRR2B', 'SPRR2D', 'SPRR2E', 'SPRR2G', 'SRP14', 'SSR4', 'SUB1', 'TACSTD2', 'TAGLN2', 'TMA7', 'TMBIM6', 'TMEM45A', 'TMSB10', 'TMSB4X', 'TOMM7', 'TPI1', 'TPT1', 'TRIM29', 'TSPO', 'TUBA1B', 'TUBA1C', 'TUBB', 'TUBB4B', 'TXN', 'TXNIP', 'TYMP', 'UBA52', 'UBB', 'UBC', 'UBE2D3', 'UBL5', 'UQCR10', 'UQCR11', 'UQCRB', 'UQCRQ', 'VIM', 'YBX1', 'YBX3', 'YWHAB', 'YWHAZ', 'ZFP36L1', 'ZFP36L2'
Lung	'A2M', 'ACADVL', 'ACTA2', 'ACTG1', 'ACTG2', 'ACTN4', 'ADIRF', 'AEBP1', 'AGR2', 'AHNAK', 'ALDH1A1', 'ANXA1', 'ANXA11', 'ANXA2', 'ANXA5', 'APLP2', 'APOD', 'AQP1', 'AQP3', 'ARF1', 'ARHGDIA', 'ATF4', 'ATP5F1A', 'ATP5F1B', 'ATP5IF1', 'ATP5MC2', 'ATP5ME', 'ATP5MG', 'ATP6V0B', 'AZGP1', 'B2M', 'BGN', 'BPIFA1', 'BPIFB1', 'BPIFB2', 'BSG', 'C11orf96', 'C1QA', 'C1S', 'C3', 'C9orf24', 'CALM1', 'CALM2', 'CALR', 'CANX', 'CAPS', 'CD151', 'CD24', 'CD59', 'CD63', 'CD81', 'CD9', 'CDC42', 'CEBPB', 'CFD', 'CHCHD2', 'CIB1', 'CKB', 'CLU', 'COL1A1', 'COL1A2', 'COL3A1', 'COL6A1', 'COL6A2', 'COX5B', 'COX6A1', 'COX6B1', 'COX6C', 'COX7A2', 'COX7C', 'COX8A', 'CRIP2', 'CSRP1', 'CST3', 'CSTB', 'CTNNA1', 'CTSB', 'CTSC', 'CTSD', 'CTSH', 'CXCL17', 'CYB5R3', 'CYBA', 'DCN', 'DDIT4', 'DDX5', 'DES', 'DHCR24', 'DMBT1', 'DUSP1', 'DYNLL1', 'EDF1', 'EEF1A1', 'EEF1D', 'EIF1', 'EIF4B', 'EIF5A', 'ELF3', 'ELOB', 'EPAS1', 'EZR', 'FBLN1', 'FCGBP', 'FLNA', 'FN1', 'FOS', 'FTH1', 'FTL', 'FXYD3', 'GAPDH', 'GLUL', 'GPX3', 'GPX4', 'GRN', 'GSTP1', 'GUK1', 'HBA1', 'HBA2', 'HINT1', 'HLA-B', 'HLA-C', 'HLA-DRA', 'HLA-DRB1', 'HLA-E', 'HMGB1', 'HMGN2', 'HNRNPA2B1', 'HNRNPC', 'HNRNPH1', 'HNRNPK', 'HSBP1', 'HSPA1A', 'HSPA5', 'HSPA8', 'HSPB1', 'IFITM2', 'IFITM3', 'IGFBP4', 'IGFBP5', 'IGFBP6', 'IGFBP7', 'IGHA1', 'IGHG1', 'IGHG3', 'IGHM', 'IGKC', 'IGLC2', 'IGLC3', 'ITGB1', 'ITM2B', 'JCHAIN', 'JUND', 'KRT15', 'KRT17', 'KRT19', 'KRT7', 'LAPTM4A', 'LCN2', 'LGALS1', 'LGALS3', 'LMNA', 'LTF', 'LUM', 'LYZ', 'MALAT1', 'METTL7A', 'MFGE8', 'MGP', 'MGST1', 'MORF4L1', 'MSMB', 'MUC1', 'MUC4', 'MUC5AC', 'MUC5B', 'MYH11', 'MYH9', 'MYL12A', 'MYL12B', 'MYL9', 'NACA', 'NAPSA', 'NBL1', 'NDUFA13', 'NDUFA4', 'NDUFB1', 'NEAT1', 'NNMT', 'NOP53', 'NPC2', 'NPM1', 'NUPR1', 'P4HB', 'PABPC1', 'PCBP1', 'PCBP2', 'PDIA3', 'PECAM1', 'PERP', 'PGC', 'PGK1', 'PIP', 'PKM', 'PLA2G2A', 'PLXNB2', 'PPDPF', 'PPP1CB', 'PRB3', 'PRB4', 'PRDX1', 'PRH2', 'PRKAR1A', 'PRR4', 'PRSS23', 'PSAP', 'PTMA', 'PTMS', 'QSOX1', 'RHOA', 'RHOB', 'RHOC', 'RNASE1', 'RSPH1', 'S100A10', 'S100A11', 'S100A2', 'S100A9', 'S100P', 'SAA1', 'SAA2', 'SAMHD1', 'SAT1', 'SCGB1A1', 'SCGB3A1', 'SDC4', 'SELENOP', 'SERF2', 'SERP1', 'SERPINA1', 'SERPINB3', 'SFTPA1', 'SFTPA2', 'SFTPB', 'SFTPC', 'SH3BGRL3', 'SKP1', 'SLC34A2', 'SLC44A4', 'SLPI', 'SMIM22', 'SNHG25', 'SOD1', 'SPARC', 'SPARCL1', 'SQSTM1', 'SRP14', 'SSR4', 'STOM', 'TACSTD2', 'TAGLN', 'TAGLN2', 'TAPBP', 'TFF3', 'TGM2', 'TIMP1', 'TIMP2', 'TIMP3', 'TMA7', 'TMEM59', 'TMSB4X', 'TPI1', 'TPM2', 'TPM4', 'TPPP3', 'TPT1', 'TRIR', 'TSC22D1', 'TSPAN1', 'TSPAN3', 'TSPO', 'TUBA1A', 'TUBA1B', 'TUBB', 'TUBB4B', 'TXN', 'TYMP', 'UBB', 'UBC', 'UBL5', 'UQCR11', 'UQCRQ', 'VAMP8', 'VIM', 'VWF', 'WFDC2', 'YBX1', 'YWHAE', 'ZFP36', 'ZFP36L1', 'ZG16B'

Figure 8. HVG gene selection in Skin and Lung

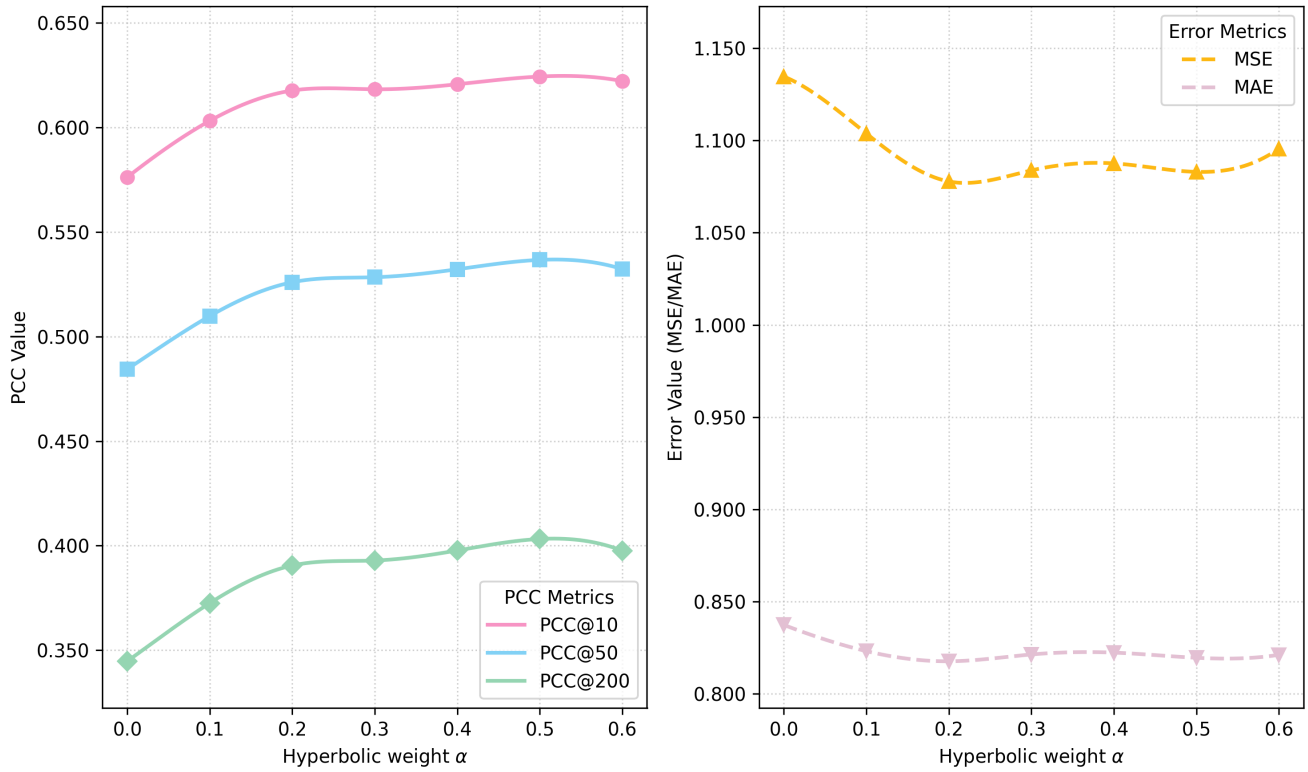

Figure 9. Sensitivity analysis on hyperbolic loss weight α

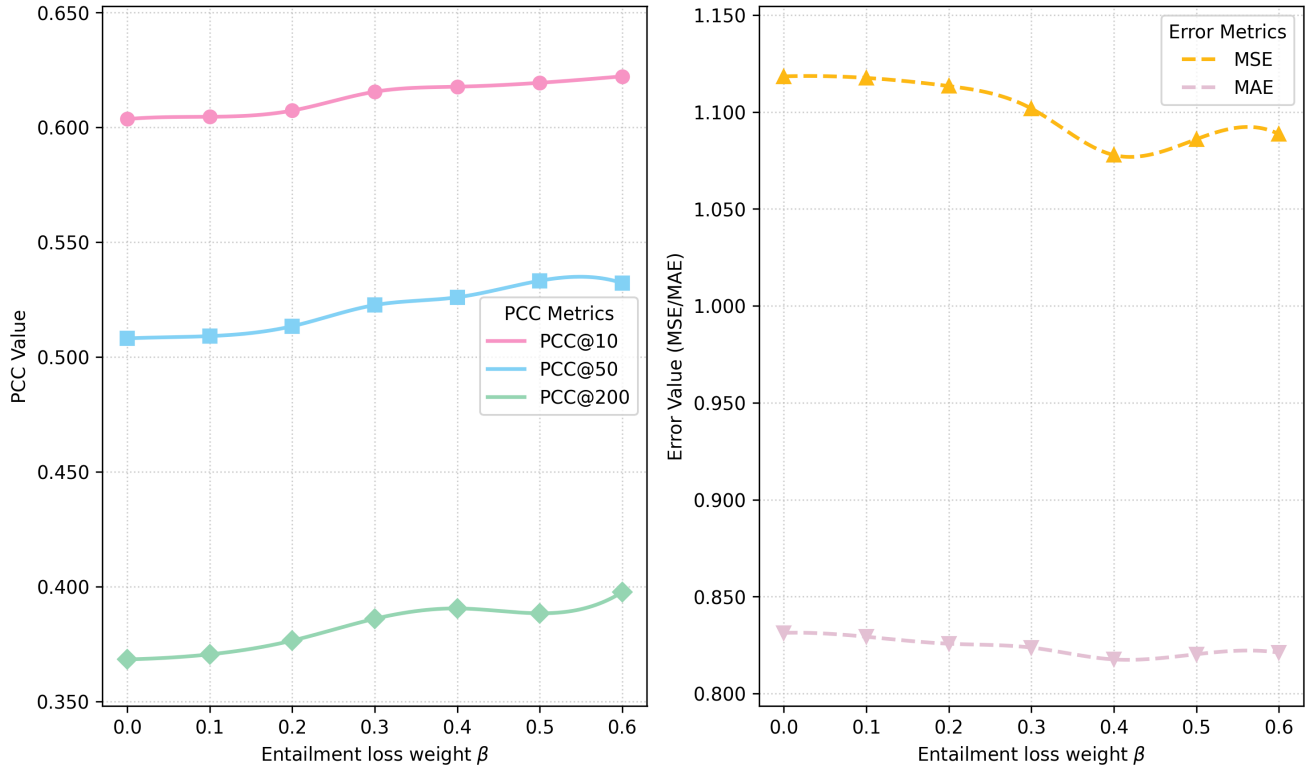

Figure 10. Sensitivity analysis on entailment loss weight β

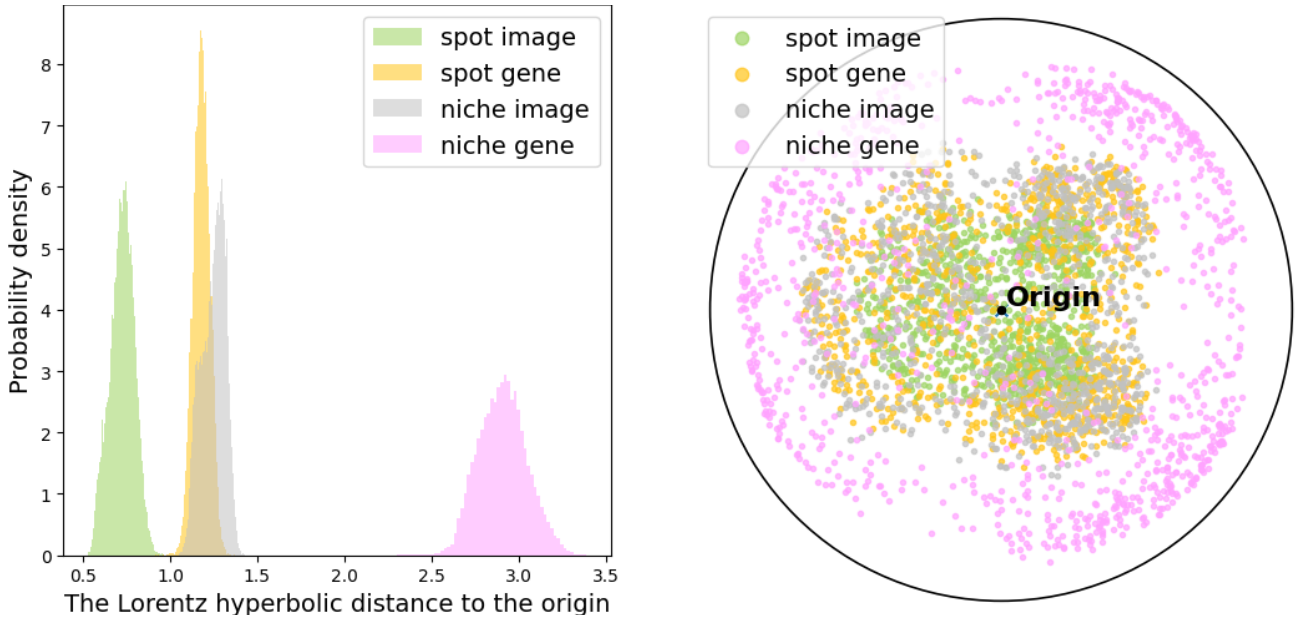

(a) Distance-to-origin distribution

(b) Visualization of the latent space

Figure 11. Visualizing the learned hyperbolic space

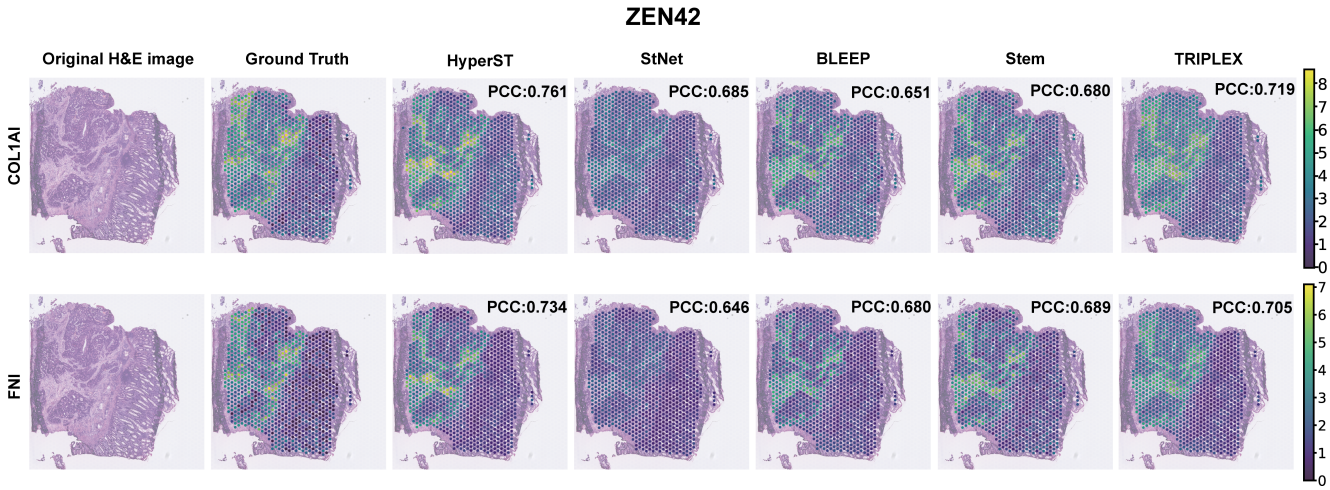

Figure 12. Visualization of COL1A1 and FN1 gene predictions in the ZEN42 sample from the Colorectum dataset. We present the PCC values comparing the ground truth with the gene expression predictions generated by each model.

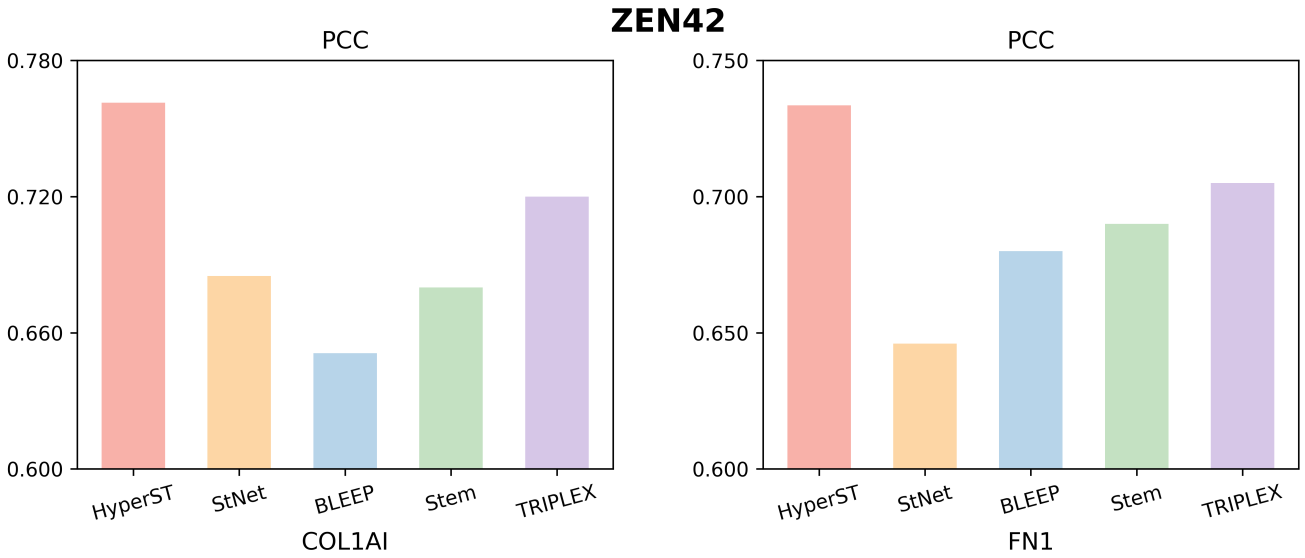

Figure 13. PCC comparison of COL1A1 and FN1 gene predictions (Higher PCC reflects greater accuracy)

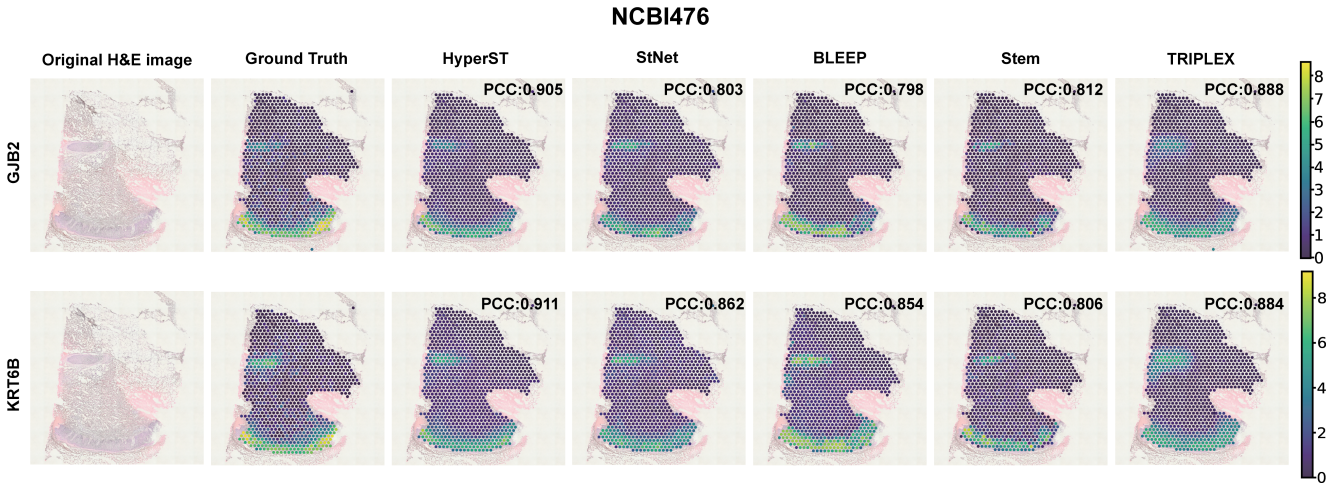

Figure 14. Visualization of GJB2 and KRT6B gene predictions in the NCBI476 sample from the Skin dataset. We present the PCC values comparing the ground truth with the gene expression predictions generated by each model.

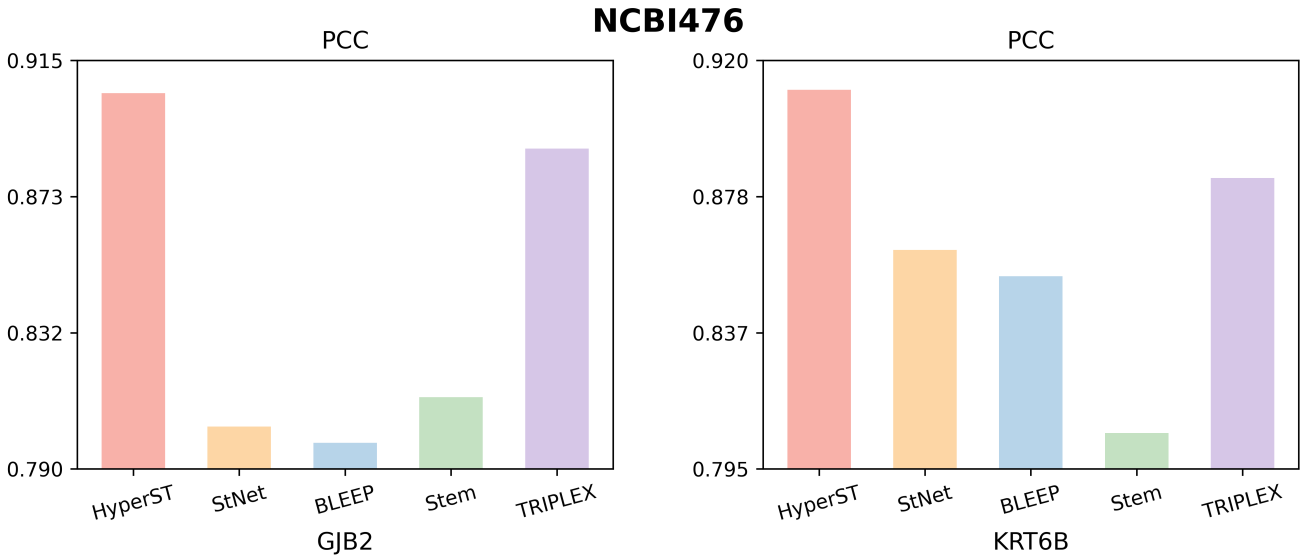

Figure 15. PCC comparison of GJB2 and KRT6B gene predictions (Higher PCC reflects greater accuracy)

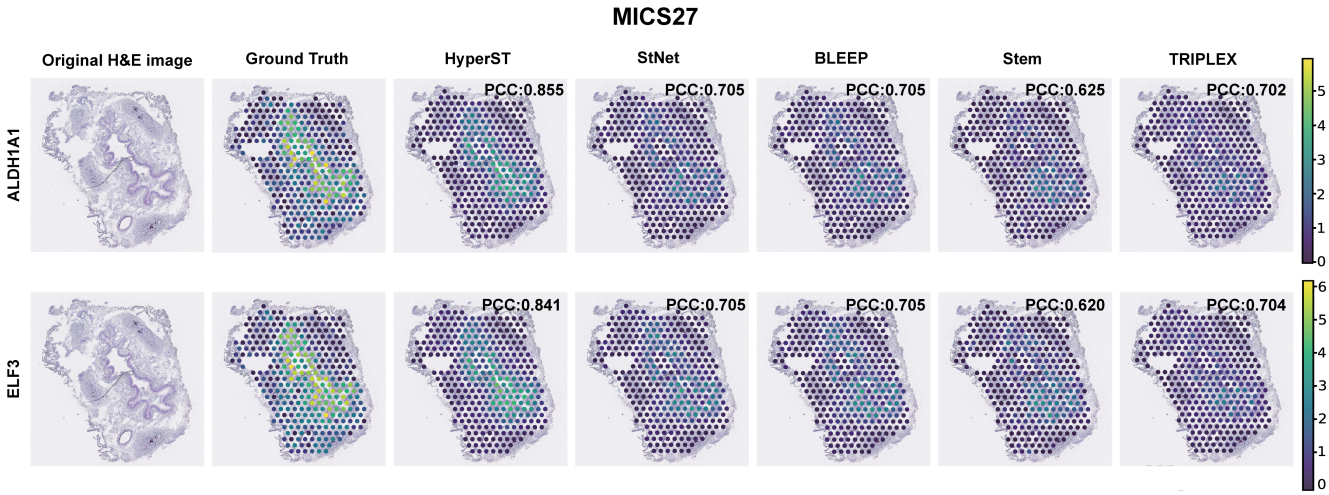

Figure 16. Visualization of ALDH1A1 and ELF3 gene predictions in the MICS27 sample from the Lung dataset. We present the PCC values comparing the ground truth with the gene expression predictions generated by each model.

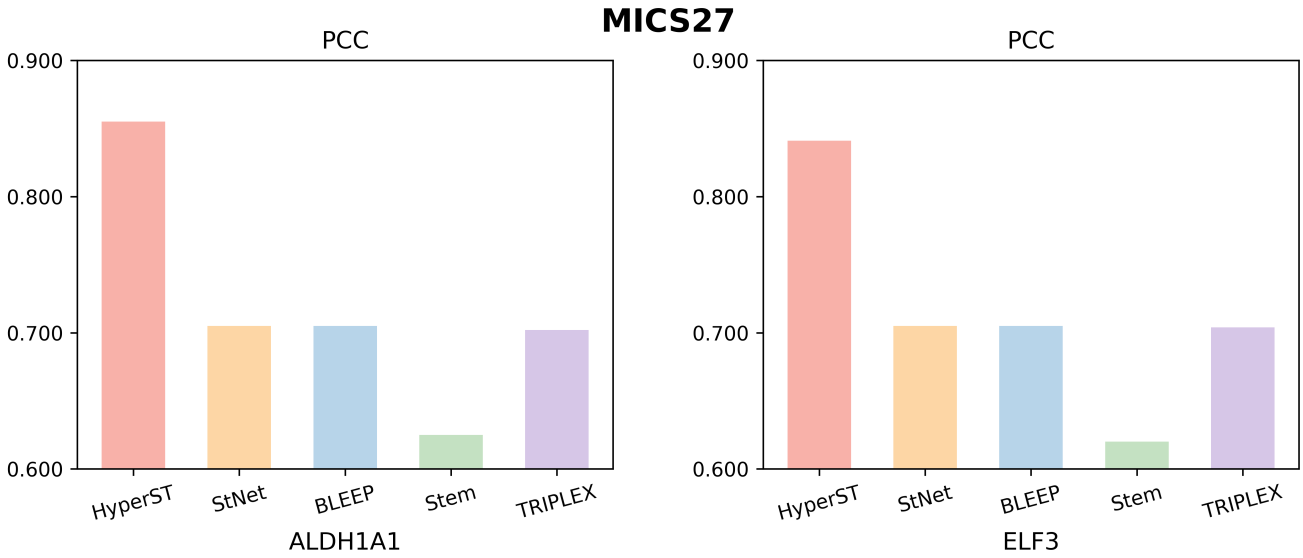

Figure 17. PCC comparison of ALDH1A1 and ELF3 gene predictions (Higher PCC reflects greater accuracy)

References

[1] Victor Hugo Canela, William S Bowen, Ricardo Melo Ferreira, Farooq Syed, James E Lingeman, Angela R Sabo, Daria Barwinska, Seth Winfree, Blue B Lake, Ying-Hua Cheng, et al. A spatially anchored transcriptomic atlas of the human kidney papilla identifies significant immune injury in patients with stone disease. *Nature communications*, 14(1):4140, 2023. 2

[2] Richard J Chen, Tong Ding, Ming Y Lu, Drew FK Williamson, Guillaume Jaume, Andrew H Song, Bowen Chen, Andrew Zhang, Daniel Shao, Muhammad Shaban, et al. Towards a general-purpose foundation model for computational pathology. *Nature Medicine*, 30(3):850–862, 2024. 3

[3] Youngmin Chung, Ji Hun Ha, Kyeong Chan Im, and Joo Sang Lee. Accurate Spatial Gene Expression Prediction by Integrating Multi-Resolution Features. In *CVPR*, pages 11591–11600, 2024. 1

[4] Erez Cohen, Craig N Johnson, Rachael Wasikowski, Allison C Billi, Lam C Tsoi, J Michelle Kahlenberg, Johann E Gudjonsson, and Pierre A Coulombe. Significance of stress keratin expression in normal and diseased epithelia. *iScience*, 27(2), 2024. 5

[5] Karan Desai, Maximilian Nickel, Tanmay Rajpurohit, et al. Hyperbolic Image-text Representations. In *International Conference on Machine Learning*, pages 7694–7731. PMLR, 2023. 1, 2

[6] Katey SS Enfield, Erin A Marshall, Christine Anderson, Kevin W Ng, Sara Rahmati, Zhaolin Xu, Megan Fuller, Katy Milne, Daniel Lu, Rocky Shi, et al. Epithelial tumor suppressor ELF3 is a lineage-specific amplified oncogene in lung adenocarcinoma. *Nature communications*, 10(1):5438, 2019. 5

[7] Bryan He, Ludvig Bergenstråhle, Linnea Stenbeck, Abubakar Abid, Alma Andersson, Åke Borg, Jonas Maaskola, Joakim Lundeberg, and James Zou. Integrating spatial gene expression and breast tumour morphology via deep learning. *Nature biomedical engineering*, 4(8):827–834, 2020. 1

[8] Blue B Lake, Rajasree Menon, Seth Winfree, Qiwen Hu, Ricardo Melo Ferreira, Kian Kalhor, Daria Barwinska, Edgar A Otto, Michael Ferkowicz, Dinh Diep, et al. An atlas of healthy and injured cell states and niches in the human kidney. *Nature*, 619(7970):585–594, 2023. 2

[9] Jonathan L. Levinsohn, Jennifer M. McNiff, Richard J. Antaya, and Keith A. Choate. A Somatic p.G45E GJB2 Mutation Causing Porokeratotic Eccrine Ostial and Dermal Duct Nevus. *JAMA dermatology*, 151(6):638–641, 2015. 5

[10] Xiao Li, Liyan Wan, Jian Geng, Chin-Lee Wu, and Xiaoyan Bai. Aldehyde Dehydrogenase 1A1 Possesses Stem-Like Properties and Predicts Lung Cancer Patient Outcome. *Journal of Thoracic Oncology*, 7(8):1235–1245, 2012. 5

[11] Ming Y Lu, Bowen Chen, Drew FK Williamson, Richard J Chen, Ivy Liang, Tong Ding, Guillaume Jaume, Igor Odintsov, Long Phi Le, Georg Gerber, et al. A visual-language foundation model for computational pathology. *Nature Medicine*, 30 (3):863–874, 2024. 3

[12] Elo Madissoon, Amanda J Oliver, Vitalii Kleshchevnikov, et al. A spatially resolved atlas of the human lung characterizes a gland-associated immune niche. *Nature genetics*, 55 (1):66–77, 2023. 2

[13] Maxime Oquab, Timothée Darcet, Théo Moutakanni, Huy Vo, Marc Szafraniec, Vasil Khalidov, Pierre Fernandez, Daniel Haziza, Francisco Massa, Alaaeldin El-Nouby, et al. Dinov2: Learning robust visual features without supervision. *arXiv preprint arXiv:2304.07193*, 2023. 3

[14] Alec Radford, Jong Wook Kim, Chris Hallacy, Aditya Ramesh, Gabriel Goh, Sandhini Agarwal, Girish Sastry, Amanda Askell, Pamela Mishkin, Jack Clark, et al. Learning Transferable Visual Models From Natural Language Supervision. In *International conference on machine learning*, pages 8748–8763. PMLR, 2021. 2

[15] Alexander Schäbitz, C Hillig, M Mubarak, Manja Jargosch, Ali Farnoud, Emanuele Scala, Nils Kurzen, Anna Caroline Pilz, Nayanika Bhalla, Jenny Thomas, et al. Spatial transcriptomics landscape of lesions from non-communicable inflammatory skin diseases. *Nature Communications*, 13(1): 7729, 2022. 2

[16] Yang Sun, Chunlin Zhao, Yanwei Ye, Zhen Wang, Yuanhang He, Yulin Li, and Haoxun Mao. High expression of fibronectin 1 indicates poor prognosis in gastric cancer. *Oncology Letters*, 19(1):93–102, 2020. 5

[17] Alberto Valdeolivas, Bettina Amberg, Nicolas Giroud, Marion Richardson, Eric JC Gálvez, Solveig Badillo, Alice Julien-Laferrière, Demeter Túrós, Lena Voith von Voithenberg, Isabelle Wells, et al. Profiling the heterogeneity of colorectal cancer consensus molecular subtypes using spatial transcriptomics. *NPJ precision oncology*, 8(1):10, 2024. 2

[18] Ronald Xie, Kuan Pang, Sai Chung, Catia Perciani, Sonya MacParland, Bo Wang, and Gary Bader. Spatially Resolved Gene Expression Prediction from Histology Images via Bimodal Contrastive Learning. In *NeurIPS*, 2023. 1, 3

[19] Hanwen Xu, Naoto Usuyama, Jaspreet Bagga, Sheng Zhang, Rajesh Rao, Tristan Naumann, Cliff Wong, Zelalem Gero, Javier González, Yu Gu, et al. A whole-slide foundation model for digital pathology from real-world data. *Nature*, 630 (8015):181–188, 2024. 3

[20] Zheying Zhang, Yongxia Wang, Jinghang Zhang, Jiateng Zhong, and Rui Yang. COL1A1 promotes metastasis in colorectal cancer by regulating the WNT/PCP pathway. *Molecular Medicine Reports*, 17(4):5037–5042, 2018. 5

[21] Sichen Zhu, Yuchen Zhu, Molei Tao, and Peng Qiu. Diffusion Generative Modeling for Spatially Resolved Gene Expression Inference from Histology Images. In *ICLR*, 2025. 1, 3

[22] Eric Zimmermann, Eugene Vorontsov, Julian Viret, Adam Casson, Michal Zelechowski, George Shaikovski, Neil Tenenholtz, James Hall, David Klimstra, Razik Yousfi, et al. Virchow2: Scaling self-supervised mixed magnification models in pathology. *arXiv preprint arXiv:2408.00738*, 2024. 3